Frontiers of Information Technology & Electronic Engineering
www.jzus.zju.edu.cn; engineering.cae.cn; www.springerlink.com
ISSN 2095-9184 (print); ISSN 2095-9230 (online)
E-mail: jzus@zju.edu.cn

A multi-sensor-system cooperative scheduling method for ground area detection and target tracking*#

Yunpu ZHANG, Qiang FU†‡, Ganlin SHAN

Department of Electronic and Optical Engineering, Shijiazhuang Campus, Army Engineering University, Shijiazhuang 050003, China

†E-mail: fq007895@163.com

Received Mar. 27, 2022; Revision accepted Aug. 16, 2022; Crosschecked Jan. 4, 2023

Abstract: A multi-sensor-system cooperative scheduling method for multi-task collaboration is proposed in this paper. We studied the method for application in ground area detection and target tracking. The aim of sensor scheduling is to select the optimal sensors to complete the assigned combat tasks and obtain the best combat benefits. First, an area detection model was built, and the method of calculating the detection risk was proposed to quantify the detection benefits in scheduling. Then, combining the information on road constraints and the Doppler blind zone, a ground target tracking model was established, in which the posterior Carmér-Rao lower bound was applied to evaluate future tracking accuracy. Finally, an objective function was developed which considers the requirements of detection, tracking, and energy consumption control. By solving the objective function, the optimal sensor-scheduling scheme can be obtained. Simulation results showed that the proposed sensor-scheduling method can select suitable sensors to complete the required combat tasks, and provide good performance in terms of area detection, target tracking, and energy consumption control.

Key words: Sensor scheduling; Area detection; Target tracking; Road constraints; Doppler blind zone
https://doi.org/10.1631/FITEE.2200121 **CLC number:** TP212.9

1 Introduction

With the development of sensor technology, sensors have been playing an increasingly important role in military and civilian fields. Specifically, in network-centric warfare, multi-sensor systems can obtain and process a large amount of battlefield information for decision-making (Misra et al., 2015; Habibi et al., 2016). However, due to the complexity and diversity of the reconnaissance environment, the high requirements for real-time information processing, and the numerous constraints of sensor working capabilities, difficulties in multi-sensor cooperation are greatly increased (Beard et al., 2015).

Therefore, it is necessary to find an effective multi-sensor scheduling method to obtain the maximum operational benefits, and this is the topic of this paper.

Based on the division of combat tasks, different sensor-scheduling methods can be applied for area detection (Pang and Shan, 2019), target recognition (Liang, 2008), target threat assessment (Katsilieris et al., 2015), and target tracking (Chhetri et al., 2006; Shi et al., 2015; Shan and Zhang, 2017; Shan et al., 2020). Researchers are focusing on these various scheduling methods for target tracking, with the aim of obtaining the ideal tracking accuracy and reducing the system cost caused by sensor operation to produce a reasonable scheduling scheme. Note that depending on the application scenario, the system cost may consist of the sensor energy cost, sensor radiation cost, and other costs.

‡ Corresponding author

* Project supported by the Defense Pre-research Fund Project of China (No. LJ20191C020393)

Electronic supplementary materials: The online version of this article (https://doi.org/10.1631/FITEE.2200121) contains supplementary materials, which are available to authorized users

ORCID: Yunpu ZHANG, https://orcid.org/0000-0002-2300-2207; Qiang FU, https://orcid.org/0000-0003-3414-3272

However, most previous work on sensor scheduling for target tracking has focused on tracking aerial targets, while neglecting ground targets. Unlike aerial targets, ground targets are slow and maneuverable, and sensors are easily affected by ground-environment clutter and complex terrain when tracking, which makes ground tracking more difficult (Wan et al., 2018; Wang et al., 2020). Because ground targets are constrained by complex terrain, combining sensors with some terrain information, such as road information constraints (Yang et al., 2010; Oh et al., 2015; Yu et al., 2016; Zheng and Gao, 2018) and rolling terrain information (Fosbury et al., 2007; Luo et al., 2021), can improve tracking accuracy. Note that the most widely used terrain information is road information constraints, which can greatly improve the tracking accuracy of targets on roads. Meanwhile, most ground detection sensors, such as ground moving-target indicator (GMTI) radar, adopt a pulse Doppler system that can greatly improve tracking performance and reduce the influence of ground-environment clutter (Mertens and Nickel, 2011; Wu et al., 2016; Zhou et al., 2021). For Doppler sensors, the existence of the Doppler blind zone (DBZ) has become a serious obstacle for tracking. DBZ arises from the cancellation of separate moving target echoes from clutter, which can reduce the influence of clutter. However, the targets whose Doppler magnitude falls below the minimum detectable velocity (MDV) will fall into DBZ, meaning that the sensor cannot track them (Hernandez et al., 2011; Zhang and Bar-Shalom, 2011). For target tracking in the presence of DBZ, Wu et al. used sensor control (Wu et al., 2020a, 2020b) and sensor fusion techniques (Wu et al., 2021a, 2021b) to suppress the DBZ masking problem, and found that tracking performance was greatly improved. According to Wu et al. (2021b), whether the target is hidden in DBZ depends on the relative motion state of the target and the sensor, and the target is usually not hidden in the DBZ of all sensors at the same time. Therefore, sensor-scheduling techniques can be used to improve tracking performance in the presence of DBZ by selecting the sensors which are non-blind at each point in time.

Most of the above sensor-scheduling methods consider only one combat task. However, the sensor system may not be assigned only one task in real combat, so multi-task collaboration should also be considered. Specifically, when the number of targets on the battlefield is uncertain, it is also necessary to detect the areas where potential static targets are located in order to find static targets, in addition to tracking the existing moving targets.

Based on the above analysis of the literature, this paper describes a new multi-sensor-system scheduling method in which the overall combat tasks are divided into two parts: ground area detection and moving target tracking. Based on the characteristics of the ground targets, our method takes road information constraints and DBZ into account in the scheduling process. That is, the motion of the proposed ground targets may be affected by road information constraints and the tracking may be influenced by DBZ. The main contributions of this paper are as follows:

1. Establish a ground area detection model to detect potential static targets, in which the detection risk based on Bayesian risk theory is introduced to quantify the detection performance in scheduling.

2. Establish a ground moving target tracking model in the presence of road constraints and DBZ, with a corresponding target tracking algorithm. In addition, the posterior Carmér-Rao lower bound (PCRLB) is introduced to quantify the target accuracy in scheduling.

3. Establish a sensor scheduling model based on multi-tasking. The objective function is established in combination with the detection loss, tracking accuracy, and energy consumption of the sensor system.

2 Problem description

The scheduling scenario considered in this paper is shown in Fig. 1. The multi-sensor system is used to perform a reconnaissance of the ground battlefield, and the total combat tasks are divided into two parts: detection of the battlefield area where the

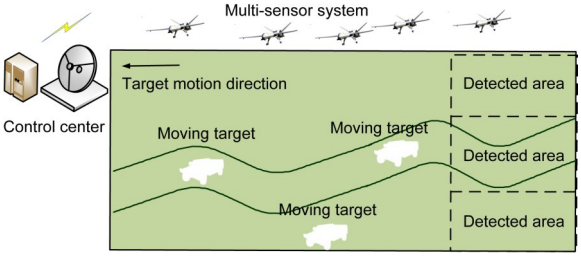

Fig. 1 Diagram of the scheduling scenario

potential static targets exist, and tracking of existing moving targets. The moving targets referred to here may move on or off the road. We assume that there are M sensors to detect S areas and track N moving targets. The sensor system has a centralized structure, with fusion processing of data and decisions on the scheduling schemes carried out by the control center.

For clarity and ease of presentation, we make the following assumptions:

1. Each sensor has two work modes, namely area detection mode and target tracking mode, but each sensor can be in only one mode at each time step.

2. The sensors use the pulse Doppler system in target tracking mode and the non-Doppler system in area detection mode.

3. To reflect the competitive relationship for assigning sensor resources between the area detection task and the target tracking task, each sensor can only detect one area or track one target at each time step.

4. The energy of the sensors is limited and their energy consumption needs to be controlled during the scheduling process.

In this paper, the scheduling scheme at time step k is denoted as $\boldsymbol{u}_k=\{\boldsymbol{a}_k,\boldsymbol{b}_k,\boldsymbol{c}_k\}$, including detection scheme $\boldsymbol{a}_k$, tracking scheme $\boldsymbol{b}_k$, and sensor-motion scheme $\boldsymbol{c}_k$. $\boldsymbol{a}_k=\left(a_k^{m,s}\right)_{M\times S}$, where $a_k^{m,s}=1$ or 0 indicates whether sensor m is to be selected to detect area s at time step k; $\boldsymbol{b}_k=\left(b_k^{m,n}\right)_{M\times N}$, where $b_k^{m,n}=1$ or 0 indicates whether sensor m is to be selected to track target n; $\boldsymbol{c}_k=\left(c_k^m\right)_{M\times 1}$, where c_k^m indicates the motion direction of sensor m. Because a sensor can only detect one area or track one target at each time step, there is $\sum_{s=1}^{S}a_k^{m,s}+\sum_{n=1}^{N}b_k^{m,n}\le 1$, $m=1, 2, ..., M$.

3 Ground area detection model

3.1 Detection probability and false alarm probability

For each area where the potential static targets may exist, assume that it is large enough to hold one target. The actual state of area s at time step k is denoted as q_k^s, where $q_k^s=1$ indicates one static target in area s and $q_k^s=0$ indicates no target. Denote $w_k^{s,m}$ as the detection value of sensor m for area s at time step k. When $a_k^{m,s}=1$, $w_k^{s,m}=1$ represents that the target is detected and $w_k^{s,m}=0$ represents that no target is detected; When $a_k^{m,s}=0$, that is, sensor m is not selected to detect area s, set $w_k^{s,m}=-1$.

Therefore, the detection matrix can be written as

$$\begin{aligned}\boldsymbol{\Theta}^m&=\begin{bmatrix}1-p_{\mathrm{f}}^m & 1-p_{\mathrm{d}}^m\\ p_{\mathrm{f}}^m & p_{\mathrm{d}}^m\end{bmatrix}\\&=\begin{bmatrix}p\left(w_k^{s,m}=0\middle|q_k^s=0\right) & p\left(w_k^{s,m}=0\middle|q_k^s=1\right)\\ p\left(w_k^{s,m}=1\middle|q_k^s=0\right) & p\left(w_k^{s,m}=1\middle|q_k^s=1\right)\end{bmatrix},\end{aligned}\tag{1}$$

where p_{d}^m and p_{f}^m represent the detection probability and the false alarm probability of sensor m in the area detection mode, respectively. Note that DBZ is not considered in the detection probability mentioned in Eq. (1), which is different from that in the target tracking mode.

3.2 Target existing probability and update method

We refer to the occurrence probability of event $q_k^s=1$ as the static target existing probability, denoted as p_k^s. p_k^s is also regarded as the a priori probability at the next time step, that is, $p_{k+1|k}^s=p_k^s$. The value of p_k^s can be updated by combining p_{k-1}^s and sensor detection value $w_k^{s,m}$. At time step k, when no sensor is scheduled to detect area s, i.e., $\sum_{m=1}^{M}a_k^{m,s}=0$, there is $p_k^s=p_{k|k-1}^s=p_{k-1}^s$.

When sensor m is scheduled to detect s, p_k^s can be updated by (Wang et al., 2011)

$$p_k^s=\begin{cases}\dfrac{\left(1-p_{\mathrm{d}}^m\right)p_{k-1}^s}{p_{k-1}^s\left(1-p_{\mathrm{d}}^m\right)+\left(1-p_{k-1}^s\right)\left(1-p_{\mathrm{f}}^m\right)}, & w_k^{s,m}=0,\\ \dfrac{p_{\mathrm{d}}^m p_{k-1}^s}{p_{k-1}^s p_{\mathrm{d}}^m+\left(1-p_{k-1}^s\right)p_{\mathrm{f}}^m}, & w_k^{s,m}=1.\end{cases}\tag{2}$$

When t_{total} sensors ($\sum_{m=1}^{M}a_k^{m,s}=t_{\mathrm{total}}\ge 1$) are scheduled to detect the area, where t_0 sensors have a detection value of 0 and $t_{\mathrm{total}}-t_0$ sensors have a detection value of 1, one should group the scheduled sensors according to the detection value and number them from 1 to t_{total}. Then the corresponding update formula is

$$p_k^s=\frac{p\left(w_k^{s,1}=\ldots=w_k^{s,t_0}=0,w_k^{s,t_0+1}=\ldots=w_k^{s,t_{\text{total}}}=1\middle|q_k^s=1\right)p_{k|k-1}^s}{p\left(w_k^{s,1}=\ldots=w_k^{s,t_0}=0,w_k^{s,t_0+1}=\ldots=w_k^{s,t_{\text{total}}}=1\right)}$$
$$=\frac{\prod_{i=1}^{t_0}(1-p_{\text{d}}^{i+h})\prod_{i=1}^{t_{\text{total}}-t_0}p_{\text{d}}^i}{p_{k-1}^s\prod_{i=1}^{t_{\text{total}}-t_0}p_{\text{d}}^i\prod_{i=1}^{t_0}\left(1-p_{\text{d}}^i\right)+\left(1-p_{k-1}^s\right)\prod_{i=1}^{t_{\text{total}}-t_0}p_{\text{f}}^i\prod_{i=1}^{t_0}\left(1-p_{\text{f}}^i\right)}p_{k-1}^s. \tag{3}$$

3.3 Detection judgment result and detection risk

When the control center receives the detection values from the sensors, it needs to make a judgment on whether the static target exists or not. We denote hypotheses $H_k^{s,0}$ and $H_k^{s,1}$ as the judgment result that there is no target or one target in s, respectively. Based on Bayesian risk theory, the minimum risk decision is introduced here to obtain the judgment result, which can minimize the loss caused by the wrong judgment (Wang et al., 2011). Note that we define the risk as the product of the probability of an event and the loss after the event. Then, the loss matrix of detection is given as

$$\mathfrak{R}_{\text{loss}}=\begin{array}{c}\\0\\1\end{array}\begin{array}{c}\begin{array}{cc}0&1\end{array}\\\begin{bmatrix}\mathfrak{R}_{00}&\mathfrak{R}_{01}\\\mathfrak{R}_{10}&\mathfrak{R}_{11}\end{bmatrix}\end{array}, \tag{4}$$

where the rows and columns of $\mathfrak{R}_{\text{loss}}$ represent the actual state and the judgment result, respectively. $\mathfrak{R}_{00}=\mathfrak{R}_{11}=0$ means that there is no loss when making the right judgment, $\mathfrak{R}_{01}$ is the false-alarm loss, and $\mathfrak{R}_{10}$ is the miss-detection loss. When miss detection occurs, we would assign fewer defensive resources to the area, which could result in a lethal attack by the enemy target. When the false alarm occurs, this misjudgment may only result in a waste of defensive resources, which represents a smaller loss than in the previous case. Therefore, we set $\mathfrak{R}_{10}\gg\mathfrak{R}_{01}$.

Combined with the above analysis, the method of the detection judgment is as follows:

1. When $\sum_{m=1}^{M}a_k^{m,s}=0$, if the judgment result is $H_k^{s,0}$, the corresponding risk can be calculated by

$$R_1\left(H_k^{s,0}\right)=\mathfrak{R}_{10}p_{k|k-1}^s+\mathfrak{R}_{00}\left(1-p_{k|k-1}^s\right)=\mathfrak{R}_{10}p_{k-1}^s. \tag{5}$$

2. When $\sum_{m=1}^{M}a_k^{m,s}=0$, if the judgment result is $H_k^{s,1}$, the corresponding risk is

$$R_2\left(H_k^{s,1}\right)=\mathfrak{R}_{11}p_{k|k-1}^s+\mathfrak{R}_{01}\left(1-p_{k|k-1}^s\right)=\mathfrak{R}_{01}\left(1-p_{k-1}^s\right). \tag{6}$$

3. When $\sum_{m=1}^{M}a_k^{m,s}=t_{\text{total}}\geq1$, if the judgment result is $H_k^{s,0}$, the corresponding risk is

$$R_3\left(H_k^{s,0}\right)=\mathfrak{R}_{00}\left(1-p_k^s\right)+\mathfrak{R}_{10}p_k^s$$
$$=\frac{\mathfrak{R}_{10}p_{k-1}^s\prod_{i=1}^{t_0}(1-p_{\text{d}}^{i+h})\prod_{i=1}^{t_{\text{total}}-t_0}p_{\text{d}}^i}{p_{k-1}^s\prod_{i=1}^{t_{\text{total}}-t_0}p_{\text{d}}^i\prod_{i=1}^{t_0}\left(1-p_{\text{d}}^i\right)+\left(1-p_{k-1}^s\right)\prod_{i=1}^{t_{\text{total}}-t_0}p_{\text{f}}^i\prod_{i=1}^{t_0}\left(1-p_{\text{f}}^i\right)}. \tag{7}$$

4. When $\sum_{m=1}^{M}a_k^{m,s}=t_{\text{total}}\geq1$, if the judgment result is $H_k^{s,1}$, the corresponding risk is

$$R_4\left(H_k^{s,1}\right)=\mathfrak{R}_{01}\left(1-p_k^s\right)+\mathfrak{R}_{11}p_k^s$$
$$=\frac{\mathfrak{R}_{01}\left(1-p_{k-1}^s\right)\prod_{i=1}^{t_{\text{total}}-t_0}p_{\text{f}}^i\prod_{i=1}^{t_0}\left(1-p_{\text{f}}^i\right)}{p_{k-1}^s\prod_{i=1}^{t_{\text{total}}-t_0}p_{\text{d}}^i\prod_{i=1}^{t_0}\left(1-p_{\text{d}}^i\right)+\left(1-p_{k-1}^s\right)\prod_{i=1}^{t_{\text{total}}-t_0}p_{\text{f}}^i\prod_{i=1}^{t_0}\left(1-p_{\text{f}}^i\right)}. \tag{8}$$

Based on the minimum risk decision, when $\sum_{m=1}^{M}a_k^{m,s}=0$, the judgment result $\hat{q}_k^s$ and the corresponding detection risk $R(\hat{q}_k^s)$ can be expressed as

$$\begin{cases}\hat{q}_k^s = \arg\min\left\{R_1\left(H_k^{s,0}\right), R_2\left(H_k^{s,1}\right)\right\},\\ R_k^s = \min\left\{R_1\left(H_k^{s,0}\right), R_2\left(H_k^{s,1}\right)\right\}.\end{cases} \tag{9}$$

Similarly, when $\sum_{m=1}^{M} a_k^{m,s}=t_{\text{total}}\geq 1$, the judgment result and the corresponding detection risk can be expressed as

$$\begin{cases}\hat{q}_k^s = \arg\min\left\{R_3\left(H_k^{s,0}\right), R_4\left(H_k^{s,1}\right)\right\},\\ R_k^s = \min\left\{R_3\left(H_k^{s,0}\right), R_4\left(H_k^{s,1}\right)\right\}.\end{cases} \tag{10}$$

3.4 Detection risk in sensor scheduling

The calculation method for detection risk after the actual detection values are obtained is given in Section 3.3. However, actual future detection values cannot be obtained when deciding the scheduling scheme. Hence, we use the expected detection values to replace the actual values and calculate the prediction $\tilde{R}_k^s$ of detection risk for deciding the scheduling scheme.

When $\sum_{m=1}^{M} a_k^{m,s} = 0$, $\tilde{R}_k^s = R_k^s$.

When $\sum_{m=1}^{M} a_k^{m,s}=t_{\text{total}}\geq 1$, the corresponding $\tilde{R}_k^s$ can be calculated as

$$\begin{aligned}\tilde{R}_k^s =& \underbrace{\sum_{w_k^{s,1}=0}^{1}\cdots\sum_{w_k^{s,t_{\text{total}}}=0}^{1}}_{t_{\text{total}}} p\left(w_k^{s,1},\ldots,w_k^{s,t_{\text{total}}}\right)\min\left\{R_3\left(H_k^{s,0}\right),\right.\\ &\left.R_4\left(H_k^{s,1}\right)\right\}\\ =& \sum_{w_k^{s,1}=0}^{1}\cdots\sum_{w_k^{s,t_{\text{total}}}=0}^{1}\min\left\{\Re_{10}p_{k-1}^s\prod_{i=1}^{t_0}\left(1-p_{\text{d}}^{i+h}\right)\prod_{i=1}^{t_{\text{total}}-t_0}p_{\text{d}}^i,\right.\\ &\left.\Re_{01}\left(1-p_{k-1}^s\right)\prod_{i=1}^{t_{\text{total}}-t_0}p_{\text{f}}^i\prod_{i=1}^{t_0}\left(1-p_{\text{f}}^i\right)\right\}.\end{aligned} \tag{11}$$

Combined with the scheduling scheme mentioned in Section 2, the prediction of the total detection risk can be written as

$$\tilde{R}\left(\boldsymbol{u}_k\right) = \sum_{s=1}^{S}\tilde{R}_k^s\left(\boldsymbol{u}_k\right), \tag{12}$$

where $\tilde{R}\left(\boldsymbol{u}_k\right)$ represents the prediction of the total detection risk under scheduling scheme $\boldsymbol{u}_k$ at time step k.

4 Ground moving target tracking model

4.1 Target-motion model

At time step k, the state of moving target n is denoted as $\boldsymbol{X}_k^n = \left[x_k^n, \dot{x}_k^n, y_k^n, \dot{y}_k^n\right]^{\text{T}}$, where x_k^n and y_k^n are the positions in the common X–Y coordinate system, and $\dot{x}_k^n$ and $\dot{y}_k^n$ are the corresponding velocities. The target motion process can be expressed by

$$\boldsymbol{X}_k^n = \boldsymbol{F}_{\eta_k}^n\boldsymbol{X}_{k-1}^n + \boldsymbol{\Gamma}_{\eta_k}^n\boldsymbol{\omega}_{\eta_k}^n, \tag{13}$$

where $\boldsymbol{F}_{\eta_k}^n$, $\boldsymbol{\Gamma}_{\eta_k}^n$, and $\boldsymbol{\omega}_{\eta_k}^n$ represent the state transition matrix, noise gain matrix, and Gaussian process noise of the actual motion model η_k, respectively. The commonly used motion models are the constant velocity (CV) model and the constant turn (CT) model (Xu et al., 2019). Note that more than one motion model is considered in the tracking problem with $\eta_k \in \boldsymbol{\eta}_{\text{model},k}^n$, where $\boldsymbol{\eta}_{\text{model},k}^n$ is the motion model set. The transition from η_{k-1} to η_k is regarded as a Markov process, with transition probability $p(\eta_k=i|\eta_k=j)$ (Xu et al., 2019). In this paper, we consider two kinds of ground moving targets, called the off-road target and the on-road target. For the off-road target, its motion is relatively free. In contrast, the motion of the on-road target is influenced by road information constraints.

4.2 Application of road information constraints in target motion

As illustrated in Fig. 2, a complex non-linear road network can be approximated as a combination of many linear road segments, which can reduce the calculation cost. When a target continuously moves on the road, its motion follows mainly

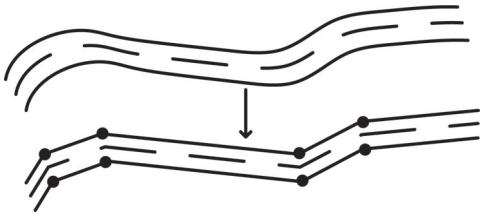

Fig. 2 Diagram of road network linearization

the road centerline without deviating largely to it (Yu et al., 2016).

The centerline equation and the direction vector of the road segment l, whose starting point is $(x^l_{\text{start}}, y^l_{\text{start}})$ and ending point is $(x^l_{\text{end}}, y^l_{\text{end}})$, are denoted as $f_l(x, y)=0$ and $\boldsymbol{\chi}_l$, respectively. If target n moves along the centerline of road segment l at time step k, the constraints on its motion state can be described as

$$\begin{cases} f_l\left(x_k^n, y_k^n\right) = 0, \\ \left\langle \left[\dot{x}_k^n, \dot{y}_k^n\right]^{\mathrm{T}}, \boldsymbol{\chi}_l \right\rangle = 0, \end{cases} \tag{14}$$

where $\left\langle \left[\dot{x}_k^n, \dot{y}_k^n\right]^{\mathrm{T}}, \boldsymbol{\chi}_l \right\rangle$ indicates the angle between $\left[\dot{x}_k^n, \dot{y}_k^n\right]^{\mathrm{T}}$ and $\boldsymbol{\chi}_l$.

Considering the deviation to the centerline caused by some disturbances, the corresponding constraints on the motion state can be described as

$$\begin{cases} \left| f_l\left(x_k^n, y_k^n\right) \right| \le \Delta d, \\ \left| \left\langle \left[\dot{x}_k^n, \dot{y}_k^n\right]^{\mathrm{T}}, \boldsymbol{\chi}_l \right\rangle \right| \le \Delta v, \end{cases} \tag{15}$$

where Δd and Δv are the deviation thresholds of the distance and velocity angle, respectively. While $\boldsymbol{X}_k^n$ satisfies constraint Eq. (15), the transition process from $\boldsymbol{X}_{k+1}^n$ to $\boldsymbol{X}_k^n$ can still be regarded as taking place on the road. At this time, the information of the road segment can be used to correct the state transition matrix $\boldsymbol{F}_{\eta_k}^n$ and the process noise $\boldsymbol{\omega}_{\eta_k}^n$.

When deviation is not considered, the CV model can be used to describe the motion of the on-road target in this paper. At this point, the state transition matrix and noise gain matrix are

$$\boldsymbol{F}_{\eta_k}^n = \begin{bmatrix} 1 & T & 0 & 0 \\ 0 & 1 & 0 & 0 \\ 0 & 0 & 1 & T \\ 0 & 0 & 0 & 1 \end{bmatrix}, \quad \boldsymbol{G}_{\eta_k}^n = \begin{bmatrix} T^2/2 & 0 \\ T & 0 \\ 0 & T^2/2 \\ 0 & T \end{bmatrix}. \tag{16}$$

When the motion of the target deviates from the road direction, to keep the target moving along the road, its motion direction should be corrected. We assume that target n is moving on segment l at time step k, the direction of target velocity is θ_k^n, the angle between road segment l and X-axis is θ_l, and the angle between l and target velocity is $\Delta\theta_k^n$. As illustrated in Fig. 3, the correction process of motion direction can be seen as a CT process with a correction angle of $\Delta\theta_k^n$. Then, the corresponding state transition matrix and noise gain matrix are

$$\begin{cases} \boldsymbol{F}_{\eta_k}^n = \begin{bmatrix} 1 & (\sin\Delta\theta_k^n)/\vartheta_k^n & 0 & \left(\cos\Delta\theta_k^n - 1\right)/\vartheta_k^n \\ 0 & \cos\Delta\theta_k^n & 0 & -\sin\Delta\theta_k^n \\ 0 & \left(1-\cos\Delta\theta_k^n\right)/\vartheta_k^n & 1 & (\sin\Delta\theta_k^n)/\vartheta_k^n \\ 0 & \sin\Delta\theta_k^n & 0 & \cos\Delta\theta_k^n \end{bmatrix}, \\ \boldsymbol{\Gamma}_{\eta_k}^n = \begin{bmatrix} T^2/2 & 0 \\ T & 0 \\ 0 & T^2/2 \\ 0 & T \end{bmatrix}, \end{cases} \tag{17}$$

where $\vartheta_k^n = \Delta\theta_k^n / T$, and T is the sampling interval.

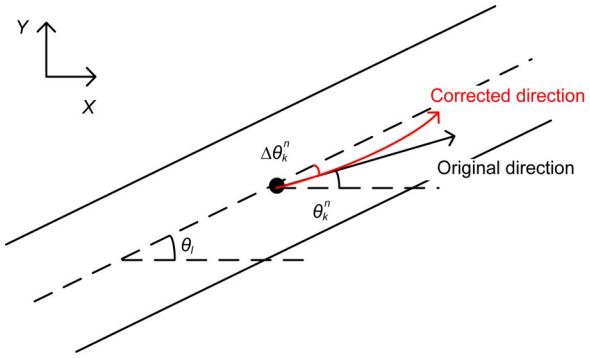

Fig. 3 Correction process of the target motion direction

When the target is moving on the road, the uncertainty of motion orthogonal to the road is much smaller than that along the road due to the presence of road constraints. We define the covariances of the process noise $\boldsymbol{\omega}(\eta_k)$ along the road and orthogonal to the road as $\sigma_{/\!/}^2$ and $\sigma_{\perp}^2$ ($\sigma_{/\!/}^2 \gg \sigma_{\perp}^2$), respectively (Zheng and Gao, 2018). After the process noise is converted to the common $X-Y$ coordinate system, the corresponding covariance matrix $\boldsymbol{Q}_{\eta_k}^n$ is written as

$$\boldsymbol{Q}_{\eta_k}^n = \begin{bmatrix} \cos\theta_l & -\sin\theta_l \\ \sin\theta_l & \cos\theta_l \end{bmatrix} \begin{bmatrix} \sigma_{/\!/}^2 & 0 \\ 0 & \sigma_{\perp}^2 \end{bmatrix} \begin{bmatrix} \cos\theta_l & -\sin\theta_l \\ \sin\theta_l & \cos\theta_l \end{bmatrix}^{\mathrm{T}}. \tag{18}$$

4.3 Sensor-measurement model and Doppler blind zone

We define the state information of sensor m as $\boldsymbol{X}_{\mathrm{s},k}^{m}=\left[x_{\mathrm{s},k}^{m},\dot{x}_{\mathrm{s},k}^{m},y_{\mathrm{s},k}^{m},\dot{y}_{\mathrm{s},k}^{m}\right]^{\mathrm{T}}$, where $x_{\mathrm{s},k}^{m}$ and $y_{\mathrm{s},k}^{m}$ are the positions, and $\dot{x}_{\mathrm{s},k}^{m}$ and $\dot{y}_{\mathrm{s},k}^{m}$ are the corresponding velocities. At each time step, the sensor transmits its state information to the control center.

The radial velocity of target n to sensor m is denoted as $\dot{r}_{k}^{m,n}$, which can be expressed as

$$\dot{r}_{k}^{m,n}=\frac{\left(\dot{x}_{k}^{n}-\dot{x}_{\mathrm{s},k}^{m}\right)\left(x_{k}^{n}-x_{\mathrm{s},k}^{m}\right)+\left(\dot{y}_{k}^{n}-\dot{y}_{\mathrm{s},k}^{m}\right)\left(y_{k}^{n}-y_{\mathrm{s},k}^{m}\right)}{\sqrt{\left(x_{k}^{n}-x_{\mathrm{s},k}^{m}\right)^{2}+\left(y_{k}^{n}-y_{\mathrm{s},k}^{m}\right)^{2}}}. \tag{19}$$

The difference between $\dot{r}_{k}^{m,n}$ and the clutter Doppler is known as clutter notch $\mathrm{nc}_{k}^{m,n}$ (Wu et al., 2016), which is used mainly to suppress clutter, but also affects the detection of low-Doppler targets. $\mathrm{nc}_{k}^{m,n}$ can be calculated as

$$\mathrm{nc}_{k}^{m,n}=\frac{\dot{x}_{k}^{n}\left(x_{k}^{n}-x_{\mathrm{s},k}^{m}\right)+\dot{y}_{k}^{n}\left(y_{k}^{n}-y_{\mathrm{s},k}^{m}\right)}{\sqrt{\left(x_{k}^{n}-x_{\mathrm{s},k}^{m}\right)^{2}+\left(y_{k}^{n}-y_{\mathrm{s},k}^{m}\right)^{2}}}. \tag{20}$$

If $\left|\mathrm{nc}_{k}^{m,n}\right|\leq$MDV, the target is hidden in DBZ, and no measurements will be obtained by the sensor.

According to Ulmke et al. (2010), considering DBZ, the sensor-detection probability can be written as

$$\tilde{p}_{\mathrm{d},k}^{m,n}=\begin{cases}p_{\mathrm{d}}^{m,n}\left\{1-\exp\left[-\left(\dfrac{\mathrm{nc}_{k}^{m,n}}{\mathrm{MDV}}\right)^{2}\ln 2\right]\right\}, & \left|\mathrm{nc}_{k}^{m,n}\right|>\mathrm{MDV},\\ 0, & \left|\mathrm{nc}_{k}^{m,n}\right|\leq\mathrm{MDV},\end{cases} \tag{21}$$

where $p_{\mathrm{d}}^{m,n}$ is the conventional detection probability in the tracking mode, which is decided by sensor parameters and the target state (Wu et al., 2016). To facilitate analysis of DBZ, it is assumed that a target not falling into DBZ will be successfully tracked by the sensor, i.e., $p_{\mathrm{d}}^{m,n}=1$.

Based on the above analysis, combined with $\tilde{p}_{\mathrm{d},k}^{m,n}$ and the sensor measurement model proposed by Li Y et al. (2009), an improved measurement model can be given as

$$\boldsymbol{Z}_{k}^{m,n}=\rho\boldsymbol{h}^{m}\left(\boldsymbol{X}_{k}^{n}\right)+\boldsymbol{v}^{m}=\begin{bmatrix}r_{k}^{m,n}\\ \varphi_{k}^{m,n}\\ \dot{r}_{k}^{m,n}\end{bmatrix}+\boldsymbol{v}^{m}$$

$$=\rho\begin{bmatrix}\sqrt{\left(x_{k}^{n}-x_{\mathrm{s},k}^{m}\right)^{2}+\left(y_{k}^{n}-y_{\mathrm{s},k}^{m}\right)}\\ \arctan\left(\dfrac{y_{k}^{n}-y_{\mathrm{s},k}^{m}}{x_{k}^{n}-x_{\mathrm{s},k}^{m}}\right)\\ \dfrac{\left(\dot{x}_{k}^{n}-\dot{x}_{\mathrm{s},k}^{m}\right)\left(x_{k}^{n}-x_{\mathrm{s},k}^{m}\right)+\left(\dot{y}_{k}^{n}-\dot{y}_{\mathrm{s},k}^{m}\right)\left(y_{k}^{n}-y_{\mathrm{s},k}^{m}\right)}{\sqrt{\left(x_{k}^{n}-x_{\mathrm{s},k}^{m}\right)^{2}+\left(y_{k}^{n}-y_{\mathrm{s},k}^{m}\right)^{2}}}\end{bmatrix}+\boldsymbol{v}^{m}, \tag{22}$$

with

$$\begin{cases}p\left(\rho=0\right)=1-\tilde{p}_{\mathrm{d},k}^{m,n},\\ p\left(\rho=1\right)=\tilde{p}_{\mathrm{d},k}^{m,n},\end{cases} \tag{23}$$

where $\boldsymbol{Z}_{k}^{m,n}$ is the actual measurement, ρ is a random number subject to the Bernoulli distribution, $\boldsymbol{h}^{m}(\boldsymbol{X}_{k}^{n})$ is the measurement equation, $\boldsymbol{v}^{m}$ is the measurement noise, and $r_{k}^{m,n}$ and $\varphi_{k}^{m,n}$ are the range and the azimuth angle of target n to sensor m, respectively.

4.4 Target tracking accuracy in sensor scheduling

In the process of sensor scheduling, the measurement of the next time step cannot be obtained. Hence, we introduce PCRLB, meaning the theoretical lower bound of the state estimation error (Song et al., 2019; Xu et al., 2019), to quantify the target tracking accuracy without using the real measurement. According to Song et al. (2019), PCRLB of target n satisfies

$$E\left\{\left[\hat{\boldsymbol{X}}_{k|k}^{n}-\boldsymbol{X}_{k}^{n}\right]\left[\hat{\boldsymbol{X}}_{k|k}^{n}-\boldsymbol{X}_{k}^{n}\right]^{\mathrm{T}}\right\}\geq\mathbf{PCRLB}_{k}^{n}, \tag{24}$$

where $\mathbf{PCRLB}_{k}^{n}$ is the PCRLB of target n at k, and $\hat{\boldsymbol{X}}_{k|k}^{n}$ is the expectation of its state estimate. The calculation methods for $\mathbf{PCRLB}_{k}^{n}$ and $\hat{\boldsymbol{X}}_{k|k}^{n}$ are shown in the supplementary materials.

The trace of the position component of $\mathbf{PCRLB}_{k}^{n}$ is selected to indicate the prediction of the target tracking accuracy in sensor scheduling, i.e.,

$$\tilde{Y}_{k}^{n}=\sqrt{\mathbf{PCRLB}_{k}^{n}(1,1)+\mathbf{PCRLB}_{k}^{n}(3,3)}. \tag{25}$$

Combined with the expression of the scheduling scheme mentioned in Section 2, the prediction of the total tracking accuracy can be written as

$$\tilde{Y}\left(\boldsymbol{u}_k\right)=\sum_{n=1}^{N}\tilde{Y}_k^n\left(\boldsymbol{u}_k\right), \tag{26}$$

where $\tilde{Y}\left(\boldsymbol{u}_k\right)$ is the prediction of the total tracking accuracy with scheduling scheme $\boldsymbol{u}_k$ at time step k.

5 Sensor-scheduling model based on multi-tasking

5.1 Energy-consumption model

Since the energy of mobile sensors is limited, it is necessary to control the energy consumption of the multi-sensor-system during sensor scheduling. In this paper, we propose a simple energy consumption model. We denote E_1^m, E_2^m, and E_3^m as the energy consumption of sensor m for area detection, target tracking, and sleeping per unit time step, respectively. If sensor m is activated to perform area detection or target tracking at k, its energy consumption is E_1^m or E_2^m, respectively. If sensor m is not activated at k, its energy consumption is E_3^m. Thus, the energy consumption of the multi-sensor-system after the scheduling scheme $\boldsymbol{u}_k$ has been implemented can be written as

$$E\left(\boldsymbol{u}_k\right)=\sum_{m=1}^{M}E^m\left(\boldsymbol{u}_k\right)=\sum_{m=1}^{M}\left[E_1^m\left(\boldsymbol{u}_k\right)+E_2^m\left(\boldsymbol{u}_k\right)+E_3^m\left(\boldsymbol{u}_k\right)\right], \tag{27}$$

where $E\left(\boldsymbol{u}_k\right)$ represents the total energy consumption in scheduling scheme $\boldsymbol{u}_k$ at time step k.

5.2 Objective function

Based on the above analysis, the performance indicators that affect the sensor-scheduling scheme are detection risk, tracking accuracy, and energy consumption. Therefore, by combining Eqs. (12), (26), and (27), we establish the following objective function in which the three performance indicators mentioned above are considered comprehensively:

$$\begin{aligned}&\Upsilon\left(\boldsymbol{u}_k\right)=\min\left[\alpha\tilde{R}\left(\boldsymbol{u}_k\right)+(1-\alpha)E\left(\boldsymbol{u}_k\right)\right]\\ &\text{s.t.}\quad \tilde{Y}_k^n\left(\boldsymbol{u}_k\right)\le Y_{\text{th}}^n,\quad n=1,2,\ldots,N,\end{aligned} \tag{28}$$

where α is the equilibrium coefficient, and Y_{th}^n is the desired tracking accuracy corresponding to target n and represents the requirement of the tracking task. The optimal sensor-scheduling scheme decided by the proposed objective function can meet the requirements of the tracking-accuracy task and achieve a balance between detection performance and energy consumption. In special cases, if no sensor meets the desired accuracy, the scheduling scheme that can obtain optimal tracking accuracy is preferred.

Note that the proposed scheduling method is myopic and does not have high computational complexity. Some traditional optimization algorithms can be used to solve the objective function, such as the particle swarm optimization algorithm (Li D et al., 2016) and artificial bee-colony algorithm (Pang and Shan, 2019).

6 Numerical simulations

In our simulations, eight sensors were dispatched to detect four areas where potential static targets might exist and track two ground moving targets, and the corresponding diagram is shown in Fig. 4. The initial position coordinates of sensors 1 to 8 were (1, 4), (1, −4), (2, 5), (2, −4), (3.2, 4.2), (3.2, −5), (4.5, 3.8), and (4.5, −5) km. The moving distance of each sensor at each time step was 60 m, and the sensor motion schemes at each time step were set to seven possible steering angles: 0°, ±30°, ±60°, and ±90°. In addition, each sensor could choose to stay at the current position. The sampling interval was 1 s, the simulation duration was 50 s, and the MDV of each sensor was 5 m/s. The parameters of all sensors are shown in Table 1.

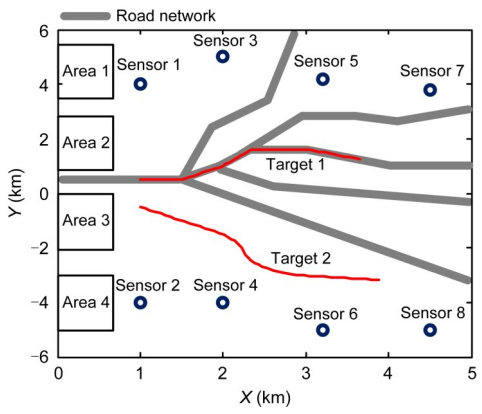

Fig. 4 Diagram of the simulation scenario

Table 1 Detection probability, false alarm probability, measurement error standard deviation, and energy consumption of all sensors

Sensor number	p_{d}^{m*}	p_{f}^{m*}	σ_r^{m**} (m)	σ_φ^{m**} (mrad)	$\sigma_{\dot{r}}^{m**}$ (m/s^2)	E_1^m (J)	E_2^m (J)	E_3^m (J)
1	99%	2%	20	5	8	22	18	0.1
2	99%	2%	20	5	8	22	18	0.1
3	96%	5%	25	10	12	19	14	0.1
4	96%	5%	25	10	12	19	14	0.1
5	93%	8%	30	15	16	15	10	0.1
6	93%	8%	30	15	16	15	10	0.1
7	90%	10%	35	15	20	12	7	0.1
8	90%	10%	35	15	20	12	7	0.1

* Area dectection mode. ** Target tracking mode

Without loss of generality, the better the detection and tracking ability, the higher the energy consumption of the sensor.

The actual states of the four areas were set as q_k^1=1, q_k^2=0, q_k^3=1, and q_k^4=0. The initial target existence probabilities of the four areas were p_0^1=30%, p_0^2=30%, p_0^3=20%, and p_0^4=50%. The loss matrix was $\Re_{\mathrm{loss}}=\begin{bmatrix}400 & 0\\ 0 & 50\end{bmatrix}$. For the detected static targets, it was assumed that they would be processed with other weapon resources.

Target 1 maintained uniform motion on the road during simulations, and had an initial position of (1, 0.5) km and an initial velocity of (50, 0) m/s. Target 2 was an off-road target with an initial position of (1, −0.5) km and an initial velocity of (60, −60) m/s. Without loss of generality, target 2 turned right with an angular velocity of 4 rad/s during 16–25 s, turned left with an angular velocity of 5 rad/s during 26–40 s, and maintained uniform motion at other times. The process-noise standard deviations of the off-road target along the X and Y directions were both 15 m, and those of the on-road target along the road and orthogonal to the road were 15 m and 2 m, respectively. The equilibrium coefficient α mentioned in Eq. (28) was 0.95, and the desired tracking accuracy of each target was 25 m (Y_{th}^1=Y_{th}^2=25 m).

To clearly analyze the performance of the proposed sensor-scheduling method (PSSM), we used two scheduling methods for comparison: the random sensor-scheduling method (RSSM), in which the scheduling scheme is selected randomly at each time step; the accuracy-based sensor-scheduling method (ABSSM), in which the scheduling scheme with optimal tracking accuracy is selected at each time step.

For each scheduling method, 100 Monte Carlo simulations were performed.

6.1 Analysis of area detection performance

The state estimations were performed based on the minimum detection risk, meaning the potential loss caused by misjudgments. The smaller the detection risk, the better the detection performance. We focused on the instantaneous and cumulative detection risk of each area with different scheduling methods, as shown in Figs. 5 and 6. It can be seen from these figures that after several times of detection for each area, the instantaneous and cumulative detection risk converged to a fixed value, indicating that the probabilities of target existence had not changed, the state estimate of each area had been determined, and the detection task had been basically completed. Comparing different scheduling methods, we can see that the detection risk with PSMM is the lowest, while the detection risks with RSMM and ABSMM are relatively high. This is because the scheduling scheme decided by PSMM takes the detection risk into account in the objective function, and can predict the risk to improve the detection performance. Meanwhile, ABSMM focuses only on optimizing the tracking accuracy, so the sensors with good detection performance are more likely to be used to complete the tracking task to the detriment of the detection task; thus, the total detection risk is the highest.

In Figs. 5 and 6, one can see that the average convergence time for detecting all areas with PSMM,

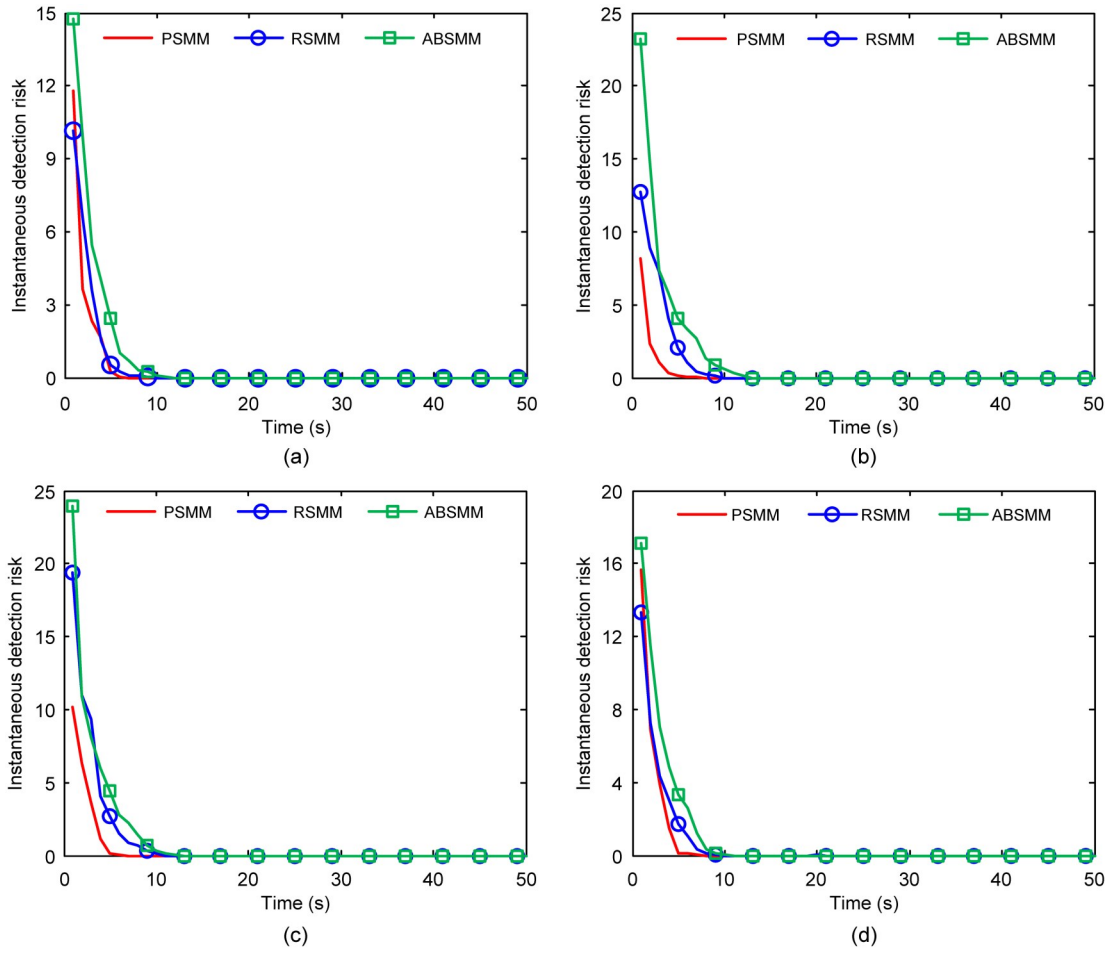

Fig. 5 Instantaneous detection risk with different scheduling methods: (a) area 1; (b) area 2; (c) area 3; (d) area 4

RSMM, and ABSMM was 6.5, 9.3, and 12.5 s, respectively. This shows that PSMM can improve the detection speed and locate the potential static target as soon as possible.

6.2 Analysis of target tracking performance

To evaluate the performance of different scheduling methods with regard to evading DBZ, we compared cumulative DBZ occurrences in 100 Monte Carlo simulations, as shown in Fig. 7. Compared with the other methods, DBZ appeared the least frequently in ABSMM. This is due to ABSMM considering only the tracking performance and thus accurately avoiding occurrence of a DBZ when deciding the scheduling scheme. The cumulative occurrence of DBZ was the highest in RSMM because this method cannot predict the states of targets and sensors. For PSMM, the corresponding cumulative occurrence of DBZ was slightly higher than that in ABSMM because PSMM also needs to take area detection and energy consumption control into account. However, it was much less than that in RSMM, indicating that PSMM performs well in evading DBZ.

To analyze target accuracy, we introduced the position root mean square error (RMSE) and root time average mean square error (RTAMSE). The position RMSE of each target with different scheduling methods can be seen in Fig. 8. We observed that the position RMSEs of each target with PSMM and ABSMM met the desired tracking-accuracy standard (Y_{th}^{1}=Y_{th}^{2}=25 m) at most simulation times, indicating that these two methods can effectively complete the target tracking task. This is because PSMM and ABSMM can select the sensors that have good accuracy to track targets by predicting the system state in the future. However, the position RMSE with RSMM was the highest and did not meet the desired tracking-accuracy standard in most cases. Note that the position RMSE of

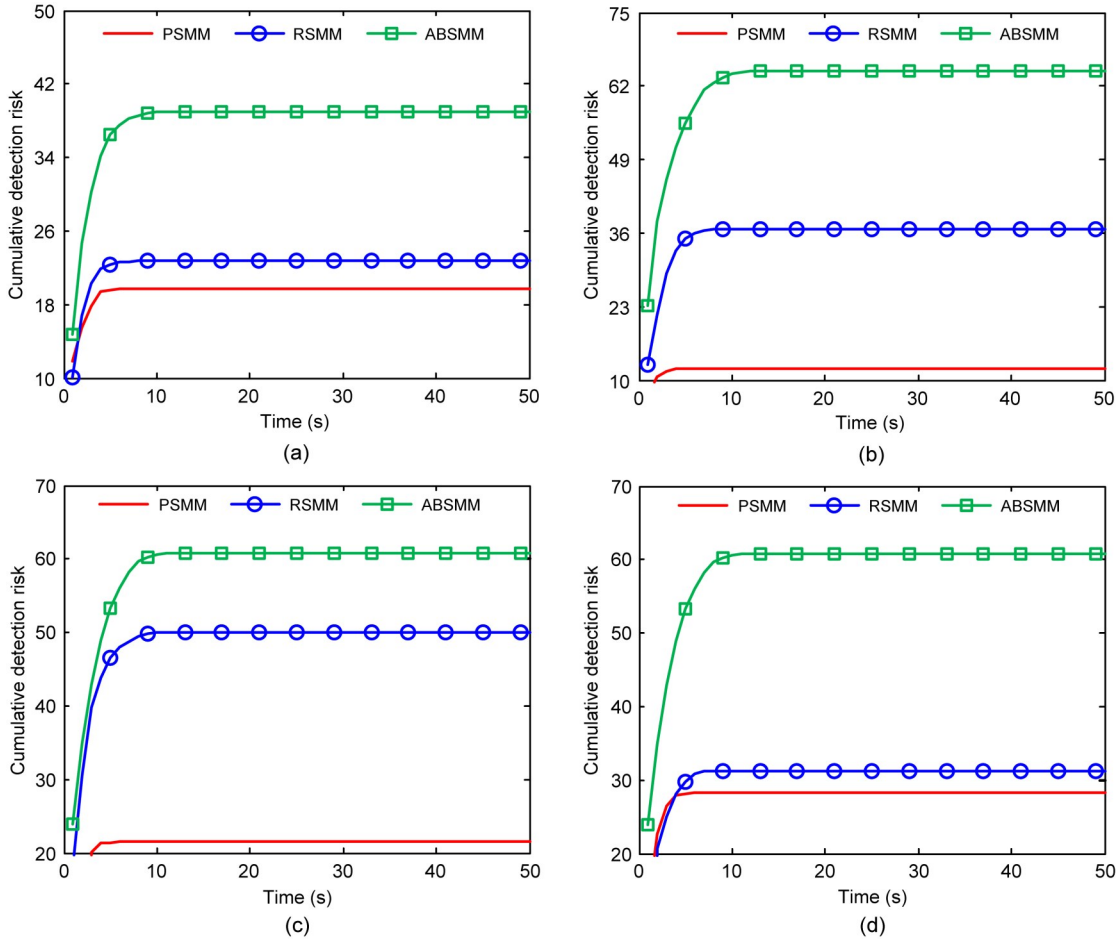

Fig. 6 Cumulative detection risk with different scheduling methods: (a) area 1; (b) area 2; (c) area 3; (d) area 4

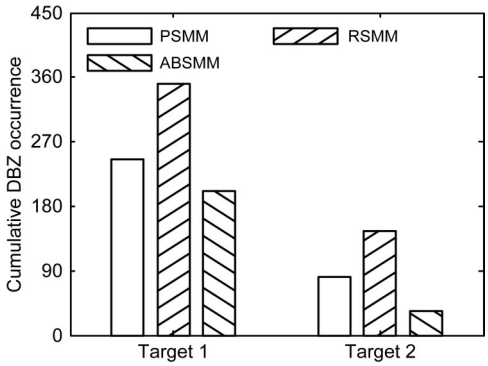

Fig. 7 Cumulative Doppler blind zone (DBZ) occurrences of each target under different scheduling methods

target 1 suddenly increased at some time points (e.g., at 10, 20, and 30 s) due to the target moving to the intersection of the road network and to the increased uncertainty of target motion.

In addition, Fig. 9 shows the position RTAMSE of each target with different scheduling methods. It is evident that RSMM has the highest tracking errors and the corresponding RTAMSE cannot meet the requirement of the tracking task. In contrast, RTAMSE in PSMM can meet the requirement (although not as good as in ABSMM) and still has good tracking performance.

6.3 Analysis of energy-consumption performance and scheduling schemes

Fig. 10 shows the cumulative energy consumption with different scheduling methods. Clearly, PSMM had the lowest energy consumption compared with the other methods, because energy consumption was considered in the objective function of sensor scheduling. This indicates that PSMM can control energy consumption and prolong the service life of the sensor system. Note that the energy consumption with ABSMM was higher than that with RSMM because ABSMM prefers to select the sensors with small measurement errors and

high energy consumption to obtain the best tracking accuracy.

Looking at these results in combination with the analysis in Sections 6.1 to 6.3, we observed that PSMM can decide effective sensor-scheduling schemes by predicting the future benefits and obtaining good performance on the area detection task, target tracking task, and energy consumption control.

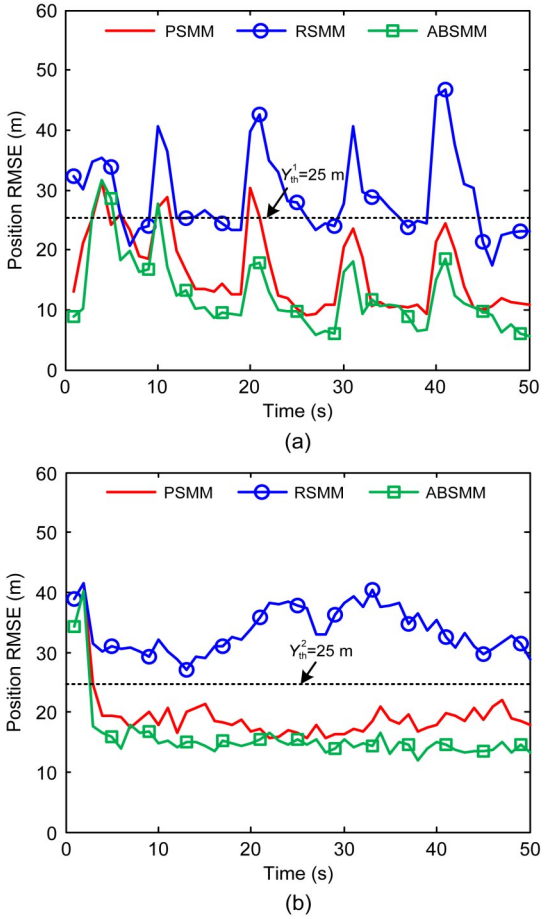

Fig. 8 Position RMSEs for each target with different scheduling methods: (a) target 1; (b) target 2

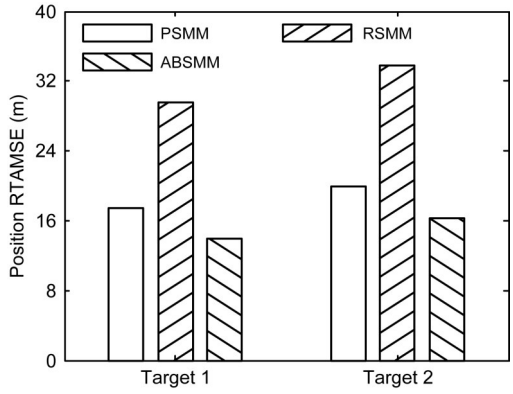

Fig. 9 Position RTAMSEs of each target with different scheduling methods

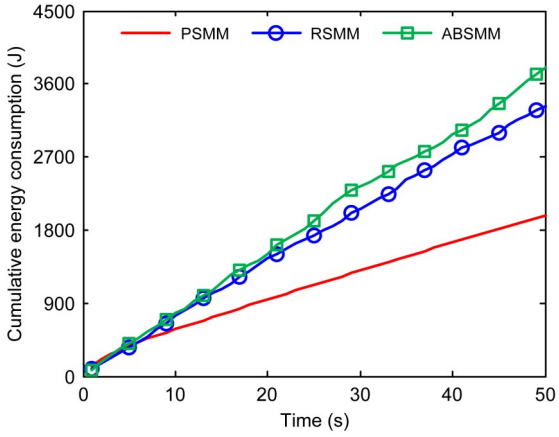

Fig. 10 Cumulative energy consumption with different scheduling methods

7 Conclusions

In this study, we developed a multi-sensor-system cooperative scheduling method for multi-task collaboration, in which the overall combat tasks were divided into ground area detection and moving target tracking, and the most suitable sensors were dynamically selected to complete the combat tasks. To describe the process of area detection, we built a detection-area model and created a benefit index called “detection risk” to quantify the detection performance of the multi-sensor system. Then, we proposed a ground-moving target tracking model in which the road constraints and Doppler blind zone problem were considered, and introduced the posterior Carmér-Rao lower bound to assess the tracking performance. In addition, using area detection, target tracking, and energy consumption, we established a sensor-optimization model based on multi-tasking to obtain optimal scheduling schemes. Simulation results showed that the proposed sensor-scheduling method is effective and can obtain an ideal combat benefit.

Contributors

Yunpu ZHANG designed the research. Qiang FU processed the data. Yunpu ZHANG drafted the paper. Ganlin SHAN helped organize the paper. Yunpu ZHANG and Qiang FU revised and finalized the paper.

Compliance with ethics guidelines

Yunpu ZHANG, Qiang FU, and Ganlin SHAN declare that they have no conflict of interest.

Data availability

The data that support the findings of this study are available from the corresponding author upon reasonable request.

References

Beard M, Vo BT, Vo BN, et al., 2015. Sensor control for multi-target tracking using Cauchy-Schwarz divergence. Proc 18th Int Conf on Information Fusion, p.937-944.

Chhetri AS, Morrell D, Papandreou-Suppappola A, 2006. Nonmyopic sensor scheduling and its efficient implementation for target tracking applications. *EURASIP J Adv Signal Process*, 2006(1):031520. https://doi.org/10.1155/ASP/2006/31520

Fosbury AM, Crassidis JL, Singh T, et al., 2007. Ground target tracking using terrain information. Proc 10th Int Conf on Information Fusion, p.1-8. https://doi.org/10.1109/ICIF.2007.4408079

Habibi J, Mahboubi H, Aghdam AG, 2016. Distributed coverage control of mobile sensor networks subject to measurement error. *IEEE Trans Autom Contr*, 61(11):3330-3343. https://doi.org/10.1109/TAC.2016.2521370

Hernandez M, Benavoli A, Graziano A, et al., 2011. Performance measures and MHT for tracking move-stop-move targets with MTI sensors. *IEEE Trans Aerosp Electron Syst*, 47(2):996-1025. https://doi.org/10.1109/TAES.2011.5751239

Katsilieris F, Driessen H, Yarovoy A, 2015. Threat-based sensor management for target tracking. *IEEE Trans Aerosp Electron Syst*, 51(4):2772-2785. https://doi.org/10.1109/TAES.2015.140052

Li D, Sun PC, Chen W, 2016. A multi-sensor management method based on particle swarm algorithm. IEEE Information Technology, Networking, Electronic and Automation Control Conf, p.766-770. https://doi.org/10.1109/ITNEC.2016.7560465

Li Y, Krakow LW, Chong EKP, et al., 2009. Approximate stochastic dynamic programming for sensor scheduling to track multiple targets. *Dig Signal Process*, 19(6):978-989. https://doi.org/10.1016/j.dsp.2007.05.004

Liang QL, 2008. Automatic target recognition using waveform diversity in radar sensor networks. *Patt Recogn Lett*, 29(3):377-381. https://doi.org/10.1016/j.patrec.2007.10.016

Luo JH, Tian YX, Chen Y, et al., 2021. Low altitude and small target tracking based on IMM L-M cubature Kalman filter. Proc 24th Int Conf on Information Fusion, p.1-8. https://doi.org/10.23919/FUSION49465.2021.9626903

Mertens M, Nickel U, 2011. GMTI tracking in the presence of Doppler and range ambiguities. Proc 14th Int Conf on Information Fusion, p.1369-1376.

Misra S, Singh A, Chatterjee S, et al., 2015. QoS-aware sensor allocation for target tracking in sensor-cloud. *Ad Hoc Netw*, 33:140-153. https://doi.org/10.1016/j.adhoc.2015.04.009

Oh H, Kim S, Tsourdos A, 2015. Road-map–assisted standoff tracking of moving ground vehicle using nonlinear model predictive control. *IEEE Trans Aerosp Electron Syst*, 51(2):975-986. https://doi.org/10.1109/TAES.2014.130688

Pang C, Shan GL, 2019. Risk-based sensor scheduling for target detection. *Comput Electron Eng*, 77:179-190. https://doi.org/10.1016/j.compeleceng.2019.05.014

Shan GL, Zhang ZN, 2017. Non-myopic sensor scheduling for low radiation risk tracking using mixed POMDP. *Trans Inst Meas Contr*, 39(2):230-243. https://doi.org/10.1177/0142331215604211

Shan GL, Xu GG, Qiao CL, 2020. A non-myopic scheduling method of radar sensors for maneuvering target tracking and radiation control. *Def Technol*, 16(1):242-250. https://doi.org/10.1016/j.dt.2019.10.001

Shi K, Chen HS, Lin Y, 2015. Probabilistic coverage based sensor scheduling for target tracking sensor networks. *Inform Sci*, 292:95-110. https://doi.org/10.1016/j.ins.2014.08.067

Song D, Tharmarasa R, Florea MC, et al., 2019. Multi-vehicle tracking with microscopic traffic flow model-based particle filtering. *Automatica*, 105:28-35. https://doi.org/10.1016/j.automatica.2019.03.016

Ulmke M, Erdinc O, Willett P, 2010. GMTI tracking via the Gaussian mixture cardinalized probability hypothesis density filter. *IEEE Trans Aerosp Electron Syst*, 46(4):1821-1833. https://doi.org/10.1109/TAES.2010.5595597

Wan KF, Gao XG, Li B, et al., 2018. Using approximate dynamic programming for multi-ESM scheduling to track ground moving targets. *J Syst Eng Electron*, 29(1):74-85. https://doi.org/10.21629/JSEE.2018.01.08

Wang Y, Hussein II, Erwin RS, 2011. Risk-based sensor management for integrated detection and estimation. American Control Conf, p.3633-3638. https://doi.org/10.1109/ACC.2011.5991348

Wang Y, Wang XG, Shan YZ, et al., 2020. Quantized genetic resampling particle filtering for vision-based ground moving target tracking. *Aerosp Sci Technol*, 103:105925. https://doi.org/10.1016/j.ast.2020.105925

Wu WH, Liu WJ, Jiang J, et al., 2016. GM-PHD filter-based multi-target tracking in the presence of Doppler blind zone. *Dig Signal Process*, 52:1-12. https://doi.org/10.1016/j.dsp.2016.01.014

Wu WH, Sun HM, Cai YC, et al., 2020a. MM-GLMB filter-based sensor control for tracking multiple maneuvering targets hidden in the Doppler blind zone. *IEEE Trans Signal Process*, 68:4555-4567. https://doi.org/10.1109/TSP.2020.3009497

Wu WH, Sun HM, Cai YC, et al., 2020b. Tracking multiple maneuvering targets hidden in the DBZ based on the MM-GLMB filter. *IEEE Trans Signal Process*, 68:2912-2924. https://doi.org/10.1109/TSP.2020.2988635

Wu WH, Sun HM, Huang ZL, et al., 2021a. Multi-GMTI fusion for Doppler blind zone suppression using PHD fusion. *Signal Process*, 183:108024. https://doi.org/10.1016/j.sigpro.2021.108024

Wu WH, Sun HM, Huang WP, et al., 2021b. Multi-GMTI decentralized tracking via consensus LMB density fusion. Int Conf on Control, Automation and Information Sciences, p.122-129.

https://doi.org/10.1109/ICCAIS52680.2021.9624574

Xu GG, Shan GL, Duan XS, 2019. Non-myopic scheduling method of mobile sensors for manoeuvring target tracking. *IET Radar Sonar Navig*, 13(11):1899-1908. https://doi.org/10.1049/iet-rsn.2019.0178

Yang C, Blasch E, Patrick J, et al., 2010. Ground target track bias estimation using opportunistic road information. IEEE National Aerospace & Electronics Conf, p.156-163. https://doi.org/10.1109/NAECON.2010.5712940

Yu M, Oh H, Chen WH, 2016. An improved multiple model particle filtering approach for manoeuvring target tracking using airborne GMTI with geographic information. *Aerosp Sci Technol*, 52:62-69. https://doi.org/10.1016/j.ast.2016.02.016

Zhang S, Bar-Shalom Y, 2011. Track segment association for GMTI tracks of evasive move-stop-move maneuvering targets. *IEEE Trans Aerosp Electron Syst*, 47(3):1899-1914. https://doi.org/10.1109/taes.2011.5937272

Zheng JH, Gao MG, 2018. Tracking ground targets with a road constraint using a GMPHD filter. *Sensors*, 18(8):2723. https://doi.org/10.3390/s18082723

Zhou GJ, Guo ZK, Li KY, et al., 2021. Motion modeling and state estimation in Range-Doppler plane. *Aerosp Sci Technol*, 115:106792. https://doi.org/10.1016/j.ast.2021.106792

List of supplementary materials

1 Target-tracking algorithm

2 Posterior Carmér-Rao lower bound

Fig. S1 Diagrams of three target location cases